

Spectroscopic evidence for a low-mass black hole in SWIFT J1753.5–0127

Vitaly V. Neustroev^{1*}, Alexandra Veledina^{1,2}, Juri Poutanen^{2,1}, Sergey V. Zharikov³, Sergey S. Tsygankov^{4,1,2}, George Sjoberg^{5,6}, Jari J. E. Kajava^{7,8,1}

¹*Astronomy Division, Department of Physics, PO Box 3000, FIN-90014 University of Oulu, Finland*

²*Tuorla Observatory, University of Turku, Väisäläntie 20, FIN-21500 Piikkiö, Finland*

³*Instituto de Astronomía, Universidad Nacional Autónoma de México, Apdo. Postal 877, Ensenada, 22800 Baja California, México*

⁴*Finnish Centre for Astronomy with ESO (FINCA), University of Turku, Väisäläntie 20, FI-21500 Piikkiö, Finland*

⁵*The George-Elma Observatory, New Mexico Skies, 9 Contentment Crest, #182, Mayhill, NM 88339, USA*

⁶*American Association of Variable Star Observers, 49 Bay State Road, Cambridge, MA 02138, USA*

⁷*European Space Astronomy Centre (ESA/ESAC), Science Operations Department, 28691 Villanueva de la Cañada, Madrid, Spain*

⁸*Nordic Optical Telescope, Apartado 474, 38700 Santa Cruz de La Palma, Spain*

Accepted 2014 September 12. Received 2014 September 10; in original form 2014 May 23

ABSTRACT

The black hole (BH) candidate SWIFT J1753.5–0127 has remained active since the onset of its 2005 outburst. Emission lines in the optical spectrum were observed at the very beginning of the outburst, but since then the spectrum has been featureless making a precise BH mass estimation impossible. Here we present results from our optical and ultraviolet (UV) observations of SWIFT J1753.5–0127 taken in 2012–2013. Our new observations show extremely broad, double-peaked emission lines in the optical and UV spectra. The optical data also show narrow absorption and emission features with nearly synchronous and significant Doppler motions. A radial velocity study of these lines which we associate with the secondary star, yields a semi-amplitude of $K_2=382 \text{ km s}^{-1}$. A time-series analysis of the spectral and photometric data revealed a possible orbital periodicity of 2.85 h, significantly shorter than the reported 3.2 h periodic signal by Zurita et al. The observed variability properties argue against a low orbital inclination angle and we present several observational arguments in favour of the BH interpretation. However, the measured radial velocity semi-amplitude of the donor star and the short orbital period imply that SWIFT J1753.5–0127 has one of the lowest measured mass function for a BH in a low-mass X-ray binary. We show that the compact object mass in excess of $5 M_\odot$ is highly improbable. Thus, SWIFT J1753.5–0127 is a BH binary that has one of the shortest orbital period and hosts probably one of the smallest stellar mass BH found to date.

Key words: accretion, accretion discs – binaries: close – stars: individual: SWIFT J1753.5–0127 – X-rays: binaries – X-rays: stars

1 INTRODUCTION

X-ray transients are a subset of the low-mass X-ray binaries (LMXBs) which spend most of their lives in a quiescent state, with typical X-ray luminosities below $10^{32} \text{ erg s}^{-1}$. Occasionally they exhibit bright X-ray and optical outbursts, which occur irregularly with intervals from a few years to decades or even longer. During the outbursts, the X-ray luminosity increases by a factor of up to $10^6 - 10^7$ in a few days and then decays back to quiescence in a few months.

SWIFT J1753.5–0127 is an X-ray transient discovered by the *Swift* Burst Alert Telescope (BAT) on 2005 May 30 as a bright vari-

able X-ray source (Palmer et al. 2005). Although the mass of the primary has not been dynamically measured, the system displays a number of characteristics that suggests the binary hosts a black hole (BH). First, the hard X-ray spectrum at the outburst peak had a maximum (in νF_ν) at $\sim 150 \text{ keV}$ (Cadolle Bel et al. 2007), while the corresponding peaks in neutron star (NS) binaries do not exceed 50 keV (Barret et al. 2000; Poutanen & Gierliński 2003; Gierliński & Poutanen 2005; Lin et al. 2007, 2010; Ibragimov & Poutanen 2009). Secondly, the X-ray spectrum of SWIFT J1753.5–0127 has significantly hardened during the decline phase, with the photon spectral index reaching values as low as $\Gamma = 1.65$ (Chiang et al. 2010), which is typical for hard state BHs, but is much smaller than that in binaries hosting a NS (Zdziarski et al. 1998; Zdziarski & Gierliński 2004; Gilfanov 2010). Thirdly, the X-ray power density

* vitaly@neustroev.net

spectrum of SWIFT J1753.5–0127 reveals a strong power suppression at frequencies above ~ 10 Hz (Durant et al. 2009; Soleri et al. 2013), unlike in NS binaries, which show significant power above ~ 500 Hz (Sunyaev & Revnivtsev 2000). Moreover, temporal analysis of the *RXTE* data (Morgan et al. 2005) revealed the presence of the low-frequency quasi-periodic oscillations (QPOs) with a shape typically seen in the BH candidates (type C QPO, see Belloni et al. 2011). Neither X-ray bursts nor pulsations were detected since the initial outburst further hinting towards the BH nature of the central source in the binary.

It is intriguing that 9 yr after the beginning of the outburst, SWIFT J1753.5–0127 has not yet returned to the quiescent state. This unusual behaviour has triggered an interest in the binary. Among other properties, a challenging task was to measure system parameters. Neither the mass M_1 of the primary nor even the orbital period P_{orb} is reliably measured at the moment. The optical photometry conducted by Zurita et al. (2008) and Durant et al. (2009) revealed a light curve with a complex non-sinusoidal morphology. The detected ~ 3.24 h modulations were attributed to the superhump period, which is known to be slightly longer than the orbital period P_{orb} (Patterson et al. 2005). This makes SWIFT J1753.5–0127 one of the shortest orbital period BH systems.

The most direct method of estimating the system parameters of the binary system involves optical spectroscopy, which can give the orbital radial velocity curve of the donor star and of the accretion disc around the primary compact object. A precise determination of the radial velocity amplitude of the secondary in a LMXB is of the highest importance as it allows us to set an absolute lower limit for the mass of the compact object. These measurements are usually done through the analysis of absorption spectra of the secondary. The most appropriate time to study the nature and dynamical properties of the secondary star in X-ray transients is quiescence, during which light from the star contributes significantly to the visible spectrum. Unfortunately, for the case of SWIFT J1753.5–0127 it will be a complicated task owing to the faintness of the source during a quiescent state. It is not visible in archival images and can be as faint as $V \sim 21$ mag (Cadolle Bel et al. 2007).

However, some dynamical information about the secondary star can potentially be derived even during outburst. For example, Steeghs & Casares (2002) detected a large number of very narrow emission line features from the irradiated secondary star in the persistent X-ray binary Sco X-1. Furthermore, the discovery of sharp emission components of the Bowen blend in Sco X-1 and the X-ray transient GX 339-4 caught in an outburst state allowed the determination of the primary masses (Steeghs & Casares 2002; Casares et al. 2003; Hynes et al. 2003; Muñoz-Darias et al. 2008).

No time-resolved spectroscopic studies for SWIFT J1753.5–0127 were reported to date, even though a few spectra were presented in the past. The observations near the outburst peak revealed the presence of the double-peaked $H\alpha$ and $\text{He II } \lambda 4686$ lines (Torres et al. 2005), which seemed to disappear a month later (Cadolle Bel et al. 2007). After that the object showed a rather featureless spectrum (Durant et al. 2009). Our photometric monitoring of SWIFT J1753.5–0127 revealed that in 2012 the binary has weakened by at least ~ 0.3 – 0.4 mag in comparison with the previous spectroscopic observations. This gave us grounds to suspect that the lines might have become more apparent. This motivated us to perform time-resolved spectroscopy of SWIFT J1753.5–0127 in order to attempt detection of these lines and to estimate the system parameters. Here we present a study of SWIFT J1753.5–0127 based

on our optical and ultraviolet (UV) spectroscopic observations, supported by the optical photometric monitoring.

2 OBSERVATIONS AND DATA REDUCTION

2.1 *HST* Ultraviolet Observations

We observed SWIFT J1753.5–0127 with the Cosmic Origins Spectrograph (COS) aboard *Hubble Space Telescope* (*HST*) on 2012 October 8 (PID 12919). The far-UV (FUV) spectra were collected using the low-resolution grating G140L in the 1280 Å setting. This grating covers 1260–2400 Å and 200–1170 Å on the A and B segments of the detector, respectively, with a spectral resolution of ~ 0.75 Å. The total exposure time of the observations was 1.36 h acquired over a 2.2 h time period (two orbits).

The data were analysed using PYRAF routines from STSDAS package HSTCOS (version 3.16). The data from each of the four exposures were summed to produce a single spectrum. Because of very low instrument sensitivity at shorter and longer wavelengths and the relatively low flux of the object ($f_\lambda \lesssim 2 \times 10^{-15} \text{ erg s}^{-1} \text{ cm}^{-2} \text{ Å}^{-1}$), we cut out the B segment of the spectrum at 1080–1170 Å and the A segment at 1260–2000 Å.

We also used another data set of the COS observations of SWIFT J1753.5–0127 retrieved from the Multimission Archive at STScI (MAST) and reduced in a similar way to that above. These data (PID 12039) taken in both the FUV and near-UV (NUV) channels, were obtained 6 d before our observations during five *HST* orbits, on 2012 October 2. The FUV spectra in this data set were taken with the high-resolution gratings G130M and G160M. The reduced spectra closely resemble our spectrum but are much noisier. Therefore, we did not use them for the following analysis. In the NUV region, the low-resolution grating G230L in the 2950 Å and 3360 Å settings was used, with the exposure time of ~ 0.4 h in each setting. Four NUV segments were covered (1690–2090 Å, 2120–2515 Å, 2790–3180 Å and 3205–3600 Å) providing a spectral resolution of ~ 0.8 Å. The G230L data for wavelengths longwards of 3200 Å can be strongly contaminated by second-order light and the flux calibration applied by CALCOS at these wavelengths is unreliable (Massa et al. 2010). For this reason we excluded from our analysis the segment covering the wavelength range 3205–3600 Å.

2.2 Optical time-resolved observations

The optical spectra of SWIFT J1753.5–0127 were obtained during four consecutive nights of 2013 August 6–9 at the Observatorio Astronómico Nacional (OAN SPM) in Mexico on the 2.1-m telescope. The observations were conducted with the Boller and Chivens spectrograph, equipped with a $13.5 \mu\text{m}$ (2174×2048) Marconi E2V-4240 CCD chip. A total of 54 spectra were obtained in the wavelength range of 3600–7000 Å, in the first order of a 400 line mm^{-1} grating with corresponding spectral resolution of ~ 4.5 Å measured from the night-sky lines. During the first night of observations 600 s individual exposures were taken (12 spectra), while the rest of the spectra were obtained using 900 s individual exposures. The total exposure time was 750 min that allowed us to achieve a signal-to-noise ratio (SNR) in the averaged spectrum of ~ 160 at 5200 Å.

All the nights of observations were photometric with exception for the first half of the second night (August 7) when cirrus clouds could have affected the flux level of the output spectra. The seeing ranged from 1 to 2 arcsec. The slit width of 2.5 arcsec was

Table 1. Log of optical time-resolved observations of SWIFT J1753.5–0127.

Date	HJD Start 2450000+	Telescope / Instrument	Filter / λ range (Å)	Exp.Time (s)	Number of exps.	Duration (h)
2013-Aug-06	6510.808	2.1 m / B&Ch	3600–7000	600	12	1.97
2013-Aug-07	6511.688	1.5 m / RATIR	V, i	80	140	3.78
	6511.718	2.1 m / B&Ch	3600–7000	900	12	3.66
2013-Aug-08	6512.660	2.1 m / B&Ch	3600–7000	900	18	5.15
	6512.684	1.5 m / RATIR	V, i	80	140	3.62
2013-Aug-09	6513.712	2.1 m / B&Ch	3600–7000	900	12	3.84

Table 2. Log of photometric observations of SWIFT J1753.5–0127.

Date	HJD start 2450000+	Exp. Time (s)	Duration (h)	Average Magnitudes			
				B	V	R	I
2012-Sep-21	6191.687	300	1.33	17.30±0.04	16.90±0.03	16.63±0.02	16.16±0.02
2012-Oct-03	6203.630	420	1.40	...	16.88±0.03	16.62±0.02	16.19±0.02
2012-Oct-08	6208.632	300	1.67	16.58±0.01	...
2012-Oct-09	6209.589	300	0.67	17.18±0.05	16.85±0.04	16.66±0.03	16.15±0.03
2013-Apr-12	6394.903	300	1.33	17.30±0.04	16.89±0.03	16.63±0.02	16.10±0.02
2013-Apr-16	6398.926	300	1.33	17.28±0.04	16.91±0.03	16.64±0.02	16.19±0.02
2013-Jun-19	6462.728	300	3.33	17.24±0.05	16.93±0.02	16.62±0.03	16.19±0.03
2013-Aug-09	6513.631	300	3.67	17.33±0.05	16.93±0.02	16.63±0.03	16.15±0.03
2013-Aug-10	6514.627	300	3.33	17.33±0.05	16.91±0.02	16.67±0.03	16.17±0.03
2013-Aug-11	6515.543	300	3.33	17.31±0.05	16.89±0.03	16.65±0.03	16.12±0.03
Mean				17.28±0.05	16.90±0.02	16.63±0.03	16.16±0.03

chosen to avoid slit losses due to possible imperfect pointing of the telescope. We note that because of the employed relatively wide slit, seeing and telescope pointing variations could lead to a variable slit illumination profile of the target, which in turn could lead to corresponding radial velocity shifts in the dispersed spectra. However, this should not be a significant problem since in the following analysis we use phase averaged data which show no significant spurious radial velocity shifts. In order to apply an accurate flux correction, three standard spectrophotometric stars were observed every night. They were selected from Feige 110, HZ 44, BD+33 2642 and BD+28 4211 (Oke 1990). Comparison spectra of Cu-He-Ne-Ar lamp were used for the wavelength calibration. The data reduction was performed using the IRAF environment.

During the nights of August 7 and 8, the spectroscopic observations were accompanied by photometric time-resolved observations on the Harold L. Johnson 1.5 m telescope at the same site. The observations were performed simultaneously in the Johnson V and SDSS i bands with the use of a multichannel imager RATIR (Butler et al. 2012; Watson et al. 2012). The exposure times were 80 s. The V magnitudes of the object were determined using the calibration stars reported by Zurita et al. (2008). Because of the lack of observations of photometric standard stars in the SDSS i filter, we used an arbitrary zero-point for the i measurements. Table 1 provides the journal of the optical time-resolved observations of SWIFT J1753.5–0127.

2.3 Optical and UV photometric monitoring

In order to investigate the long-term photometric behaviour and to check for the current state of the object during our spectroscopic observations, we additionally obtained several sets of multicolour

photometric data. These observations were performed from 2012 September to 2013 August at New Mexico Skies in Mayhill, New Mexico, with the 0.35-m Celestron C14 robotic telescope and an SBIG ST-10XME CCD camera with Johnson-Cousins $BV(RI)_C$ Astrodon Photometric filters. The images were usually taken in a sequence $B-V-R-I$ with exposure times of 300 s for each filter. In order to establish nightly averaged fluxes, we observed the object for several hours per night. The data reduction was performed using the IRAF environment and the software AIP4Win v. 2.4.0 (Berry & Burnell 2005). In order to improve the confidence of our measurements we aligned and summed all the nightly images for each filter and then measured the average magnitudes. We used the secondary standards found in Zurita et al. (2008) to establish the zero points. Table 2 provides a journal of the photometric observations with the measured magnitudes. We note that the VRI magnitudes obtained on 2012 October 3 are very close to the values of Froning et al. (2014) obtained a day before.

We also performed a Target of Opportunity (ToO) observation of SWIFT J1753.5–0127 in $uvw2$ filter with the UV-Optical Telescope (UVOT) onboard the *Swift* X-ray satellite (Gehrels et al. 2004) on 2012 September 19. Furthermore, we used the *Swift*/UVOT data obtained during the entire 2012 year. These observations were analysed with the *Swift* Release 3.7 software¹ together with the most recent version of the Calibration Database. The UVOT observations were reduced following the procedure described in Poole et al. (2008).

¹ <http://swift.gsfc.nasa.gov/docs/software/lheasoft/>

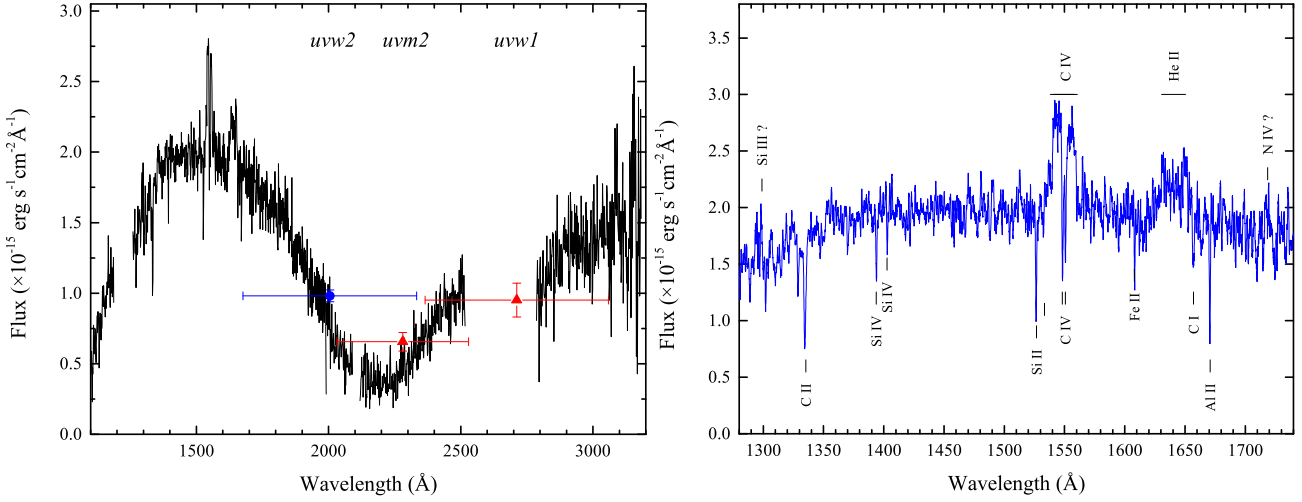


Figure 1. Left: The UV spectrum of SWIFT J1753.5–0127 uncorrected for interstellar reddening. The data have been binned to ~ 2.5 Å spectral resolution. The blue circle and red triangles show the Swift/UVOT measurements. Right: A part of the FUV spectrum containing the strongest lines and smoothed with a 20 point running boxcar to show the weaker lines.

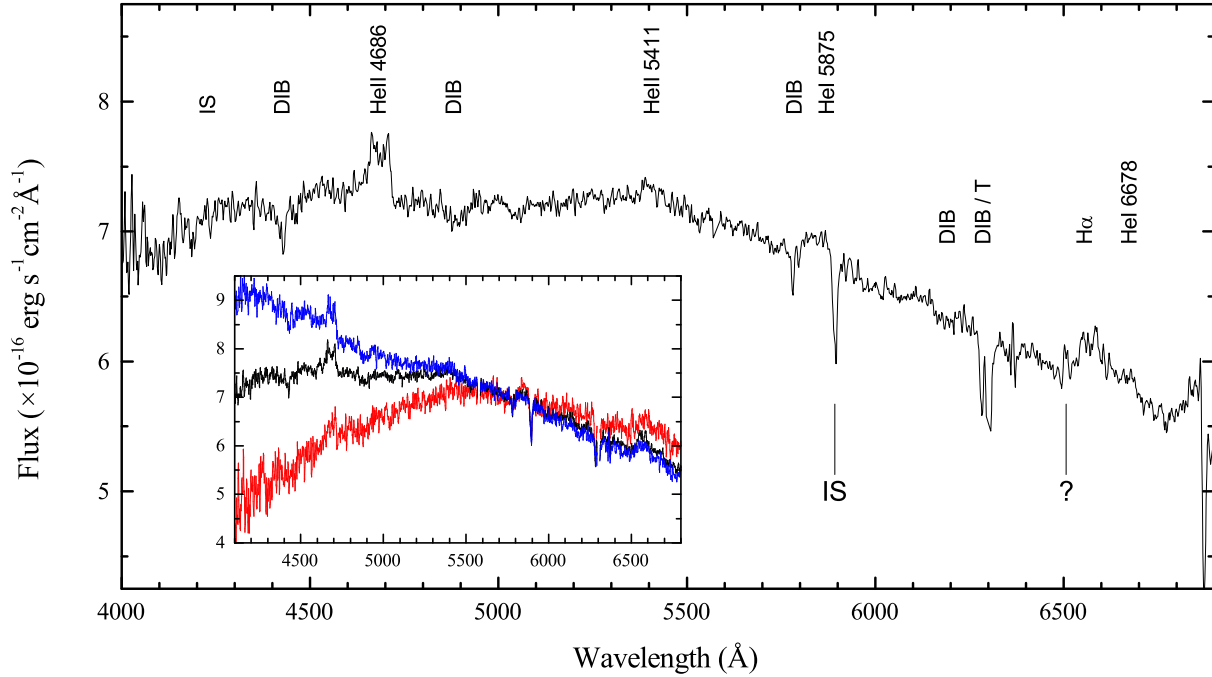


Figure 2. The averaged optical spectrum of SWIFT J1753.5–0127. The inset shows the extreme shapes of the variable continuum.

3 DATA ANALYSIS AND RESULTS

3.1 UV spectrum

The UV spectrum of SWIFT J1753.5–0127 is shown in Fig. 1 (left-hand panel). The spectrum is uncorrected for the interstellar reddening, which manifests itself in a deep absorption feature centered at 2175 Å. We also show the UVOT measurements in UV filters (*uvw1*, *uvm2*, *uvw2*). Only the *uvw2* measurements were obtained near the time of the *HST* observations, the fluxes in other UVOT filters are the average of the measurements obtained during the year 2012. The UVOT fluxes are very similar to those derived from the spectroscopy.

The UV spectrum is dominated by broad and double-peaked

emission lines of C IV $\lambda 1550$ and He II $\lambda 1640$ with no P Cyg absorption components. These properties allow us to place constraints on the orbital inclination (see Section 4.4), and on the accretion disc outer radii where the UV emission lines originate. There is also a hint of other weaker emission lines of Si III $\lambda 1298$ and N IV $\lambda 1718$. The absorption spectrum is rich in features, but all these absorption lines are very narrow and are not shifted with respect to the rest wavelength being consistent with the interstellar origin. The strongest lines are C I $\lambda 1657$, C II $\lambda 1335$, C IV ($\lambda 1548.2$, $\lambda 1550.7$), Si II ($\lambda 1527$, $\lambda 1533$), Si IV ($\lambda 1393.8$, $\lambda 1402.7$), Fe II $\lambda 1608$, Al II $\lambda 1671$. In the NUV spectrum we were unable to identify any spectral lines. A part of the FUV smoothed spectrum containing the strongest lines is shown in Fig. 1 (right-hand panel).

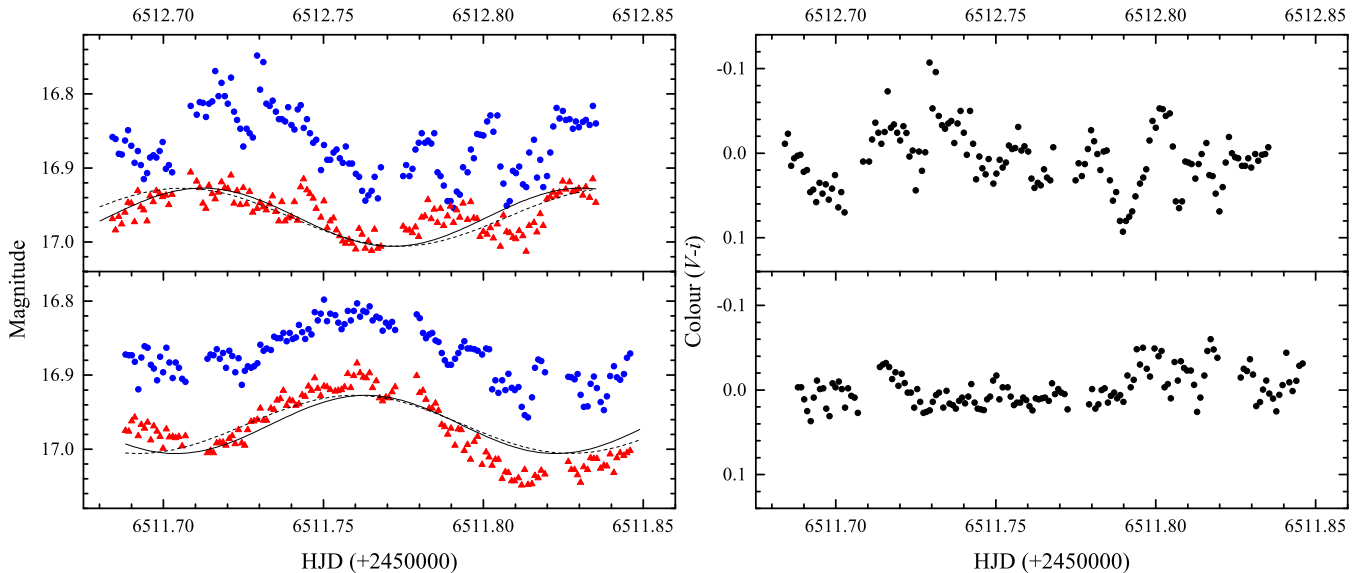


Figure 3. Left: the V (blue circles) and SDSS i -band (red triangles) light curves of SWIFT J1753.5–0127. Because of the lack of observations of photometric standard stars in the SDSS i filter, an arbitrary zero-point was used for the i -band measurements. The solid and dashed lines are sinusoidal fits to the i -band data with the period constrained to ~ 2.85 h and ~ 3.24 h, respectively. Right: the corresponding $V - i$ colour (with the linear trend subtracted for each night of observations).

3.2 Optical spectrum

The averaged optical spectrum of SWIFT J1753.5–0127 is shown in Fig. 2. It exhibits very broad double-peaked emission lines of He II $\lambda 4686$ and H α . There are also hints of He II $\lambda 5411$ and He I emission lines (5875 Å, 6678 Å) and of the Bowen blend. We also note the presence of a narrow, unidentified emission line at ~ 6507 Å. This feature seems to be real and not an artefact of the data reduction because it is present in all our subsets of observations of SWIFT J1753.5–0127, but is not seen in spectra of any other targets observed the same nights. To the best of our knowledge, the detection of a similarly weak emission line in this wavelength region was reported only for the X-ray transient GX 339–4. Soria, Wu, & Johnston (1999) identified this line with N II $\lambda 6505$. However, we doubt this identification as no other N II lines are observed in either SWIFT J1753.5–0127 or GX 339–4.

Several diffuse interstellar bands (DIB), interstellar (IS) and telluric absorption lines (T) are apparent in the spectrum. Besides them, no other absorption lines which might be identified with the secondary star are seen in this averaged spectrum. However, the time-resolved spectra reveal a few narrow absorption and emission features which show significant sinusoidal Doppler shifts. We discuss these features in Section 3.4.

The continuum in the averaged spectrum has a broken-line shape with a knee around 5400 Å, somewhat similar to the WHT/ISIS spectrum obtained in 2006 June 17 (Durant et al. 2009), but in contrast to most of other spectra from early observations which could be reasonably well represented by a straight line (Cadolle Bel et al. 2007; Durant et al. 2009). A visual inspection of individual spectra has shown that the continuum shape exhibits strong variability. The slope of the shorter wavelength segment significantly varies, while the longer wavelength segment is much more stable (see the inset in Fig. 2). We checked if these variations could be caused by wavelength dependent slit losses and found no correlation with seeing and airmass. Moreover, the spectra of other variable and standard stars taken during the same nights with the same telescope/instrument did not reveal such variability

of the continuum shape. Thus, the detected variability is real and is not an artefact of the flux calibration.

In order to study the time dependence of this variability, we calculated the ratio F_{4300}/F_{6250} , where F_{4300} and F_{6250} are the fluxes averaged across the wavelength bands centered at 4300 Å and 6250 Å with the widths of 600 Å and 500 Å, respectively. This ratio is analogous to the colour $B - R$. In Section 3.3, we show that F_{4300}/F_{6250} displays a notable variability with the orbital period. In addition, there are signs in our RATIR data of another, shorter time-scale variability associated with varying continuum shape, which is stronger in the V -band than in the i -band. The corresponding peak-to-peak amplitude of the $V - i$ colour index variability is as large as ~ 0.15 mag, which is similar to the amplitude of the orbital modulation (Fig. 3). Because of the shortness of these RATIR observations we are unable to reach a firm conclusion on the periodicity of the detected variability, but the data hint towards the period of ~ 33 min. Longer multicolour observations with high enough time resolution preferably in the B and R filters should shed more light on this phenomenon. In conclusion, we note that the nightly averaged magnitudes are very stable in all the filters except for B (Table 2; see also Froning et al. 2014). The latter shows the relatively large observed scatter in magnitudes. It can naturally be explained by the optical continuum variability if it is also present on the longer time scales.

3.3 Orbital period

SWIFT J1753.5–0127 is known to show relatively strong modulations as seen in its optical light curve (Zurita et al. 2008; Durant et al. 2009), however the precise orbital period of the system is still unknown. Zurita et al. (2008) reported a determination of the modulation period to be ~ 3.24 h which they attributed to a superhump period. During our observations, a similar modulation is also clearly visible in both V and i filters (Fig. 3). There also is an apparent colour variability that is in contrast to the observations of Durant et al. (2009), during which the colours varied very little.

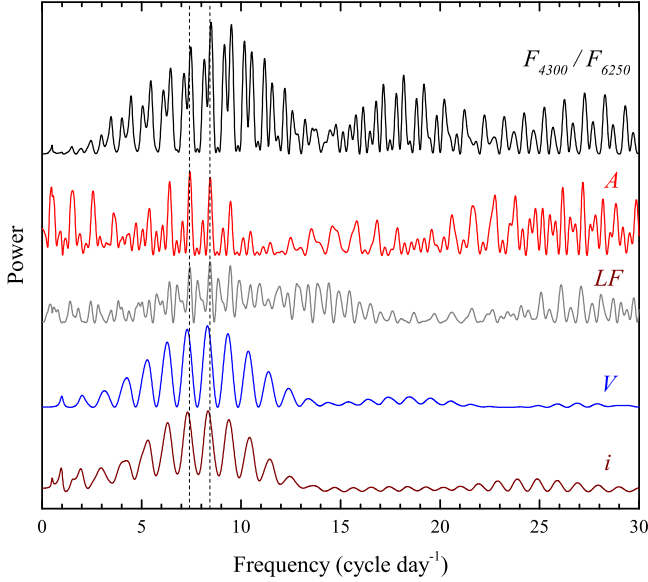


Figure 4. Power spectra of different quantities calculated from the optical photometric and spectroscopic data (see text for explanation). The vertical dashed lines mark the adopted orbital frequency of 8.41 cycle d^{-1} and the previously proposed 3.24 h period (7.41 cycle d^{-1}).

The Lomb-Scargle periodograms for the *V* and *i* RATIR photometric data show the strongest peaks at a frequency of ~ 8.4 cycle day^{-1} (Fig. 4), which is close to the 1-d alias of the period found by Zurita et al. (2008).

Besides the analysis of photometric variability, we also performed a time series analysis of our optical spectroscopic data. In addition to the colour index F_{4300}/F_{6250} introduced in Section 3.2, we also calculated additional quantities. The quantity LF (normalized line flux) is closely related to the equivalent width (EW) of He II $\lambda 4686$ and defined as the flux integrated over the wavelength range $\lambda\lambda 4645\text{--}4726$ Å divided by the averaged flux in the wavelength ranges $\lambda\lambda 4512\text{--}4612$ Å and $\lambda\lambda 4727\text{--}4827$ Å. We also introduce the asymmetry parameter *A* as the ratio of the EWs of the He II $\lambda 4686$ line on each side of the rest wavelength. This parameter is sensitive to the variations of both the radial velocity and the shape of the He II $\lambda 4686$ line profile.

The power spectra of F_{4300}/F_{6250} , *A* and *LF* are also shown in Fig. 4. Most of them are dominated by a peak at the same frequency of ~ 8.4 cycle d^{-1} , with its averaged value being 8.41 ± 0.04 cycle d^{-1} (2.85 ± 0.01 h), where the error is expressed as the standard deviation of the mean. The existence of the variability with the same period in both the photometric and spectroscopic data indicates that this is the true orbital period.

3.4 The radial velocity of the secondary star

In outburst, the optical flux from the binary system is dominated by emission from the luminous accretion disc, making the photospheric absorption lines of the donor virtually undetectable. However, closer inspection of the trailed spectrum of SWIFT J1753.5–0127 revealed hints of several narrow absorption and emission features that showed radial velocity variations with a large amplitude and in phase with each other. These weak features are more or less clearly seen only in the wavelength region with the highest SNR ($\sim 5100\text{--}5400$ Å). A few other absorption lines may also be presented in other spectral regions, though their detection is less

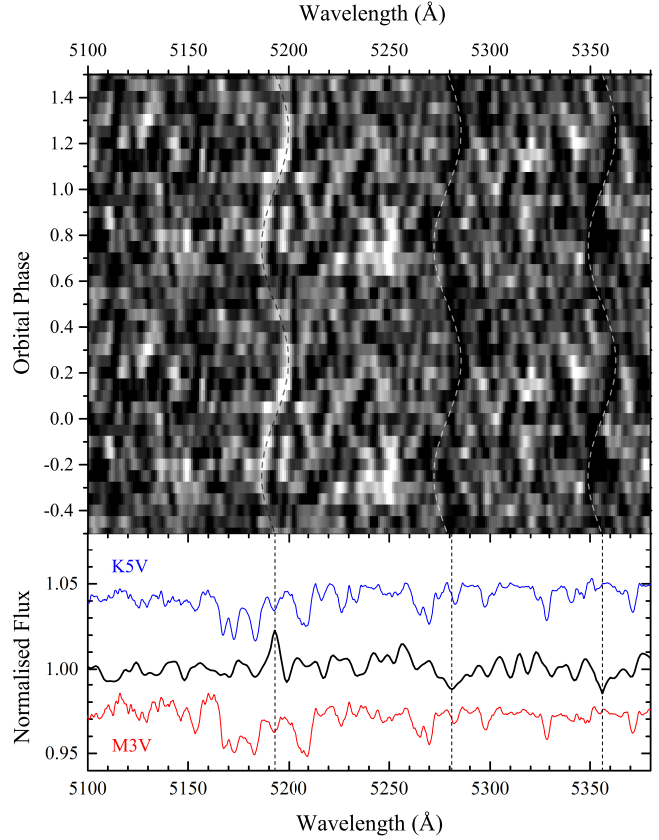


Figure 5. Top: a part of the trailed spectrum of SWIFT J1753.5–0127 showing sinusoidal trails of absorption and emission features, marked by the dashed lines. White indicates emission. Two cycles are shown for clarity. Bottom: the averaged and normalized spectrum of SWIFT J1753.5–0127, compared with two spectral standards. The spectrum of SWIFT J1753.5–0127 have been corrected for orbital motion of the secondary star.

reliable. The strongest detected lines are located at ~ 5193.0 Å, 5279.0 Å and 5356.1 Å and marked by the dashed lines in Fig. 5 (top panel). Surprisingly, their identification is unclear. This spectral region of late K- and M-type stars contains a wealth of absorption lines. Some of them can be matched with the features detected in the spectrum of SWIFT J1753.5–0127, but the absence of other expected lines stalls the identification (Fig. 5, bottom panel).

Nevertheless, the presence in the spectrum of an ensemble of spectral features with nearly synchronous and significant Doppler motions indicates their common origin which we tentatively associate with the secondary star.

In order to characterize these velocity variations, we first phased the individual spectra with the orbital period of 2.85 h and then co-added the spectra into 20 separate phase bins. We placed orbital phase zero at HJD 245 6510.8081 – the time of inferior conjunction of the secondary star (derived later in this section). The resulted phase-folded spectra have relatively high SNR of $\sim 50\text{--}70$ (at 5200 Å).

The radial velocity measurements of the donor star in LMXBs are usually obtained through cross-correlation of the absorption lines with stellar templates of similar spectral type. This method works even if the spectral features of the secondary star are not obvious in the spectrum. However, the mismatch between spectral lines of SWIFT J1753.5–0127 and the standard stars requires to use another template. Following the iterative approach described

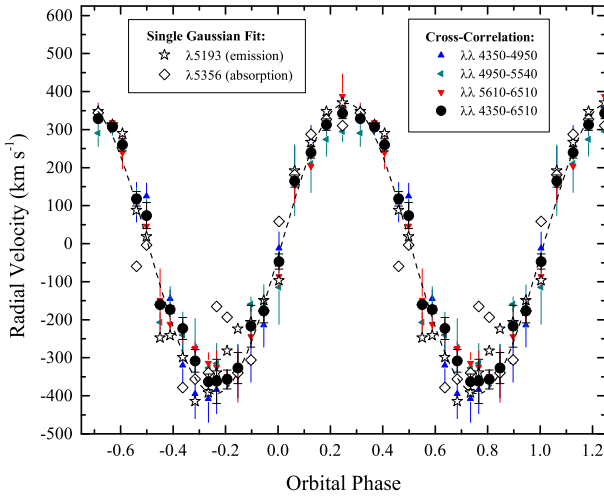


Figure 6. Radial velocities of the secondary star folded on the ephemeris from Table 4. The measurements are obtained using the cross-correlation in different wavelength ranges. It also shows the radial velocities of the lines $\lambda 5193$ Å (in emission) and $\lambda 5356$ Å (in absorption) obtained with a single Gaussian fit. Two cycles are shown for clarity.

in Neustroev & Zharikov (2008), we created the cross-correlation template spectrum from the observed spectra of the system. This approach maximizes the similarity between the template and the individual spectra to be cross-correlated.

The first step was to measure the radial velocity variations of the strongest observed lines $\lambda 5193$ Å and $\lambda 5356$ Å. The velocities were independently measured by fitting each line profile in the phase-folded spectra with a single Gaussian. The resulting radial velocity curves were then fitted with a sinusoid of the form

$$V(\phi) = \gamma - K_{2,o} \sin[2\pi(\phi - \phi_0)]. \quad (1)$$

We obtained the observed radial velocity semi-amplitude $K_{2,o}$ to be 383 ± 13 km s⁻¹ for the emission line $\lambda 5193$ Å and 349 ± 20 km s⁻¹ for the absorption line $\lambda 5356$ Å, whereas the difference between the phase zero-points ϕ_0 for these lines was found to be ~ 0.01 (Fig. 6). Using these preliminary values of $K_{2,o}$ and ϕ_0 , each individual spectrum was then shifted to correct for the orbital motion of the donor star. The cross-correlation template was then obtained by averaging shifted individual spectra.

In the next step, the phase-folded spectra of SWIFT J1753.5–0127 were cross-correlated with the template. Prior to the cross-correlation, the target and template spectra were normalised by dividing by the result of fitting a low-order spline to the continuum. In a case of noise-dominated spectra, its cross-correlation with any template may produce spurious peaks in the cross-correlation function (CCF) and the correspondingly measured radial velocities would not follow a common sine curve. Therefore, in order to test for reliability in the derived parameters, the cross-correlation was carried out in three separate wavelength regions $\lambda\lambda 4350$ – 4950 Å, $\lambda\lambda 4950$ – 5550 Å and $\lambda\lambda 5610$ – 6510 Å. To avoid the influence of the emission and the night-sky lines, the portions of the spectra around these spectral features were masked. We found that all the corresponding CCFs show strong and distinct peaks (Fig. 7). The radial velocity and its accuracy were then determined by fitting the strongest peak of each CCF with a Gaussian and a linear background. Our solutions obtained by fitting the measured radial velocities with the sinusoid (equation 1) are very similar for all three

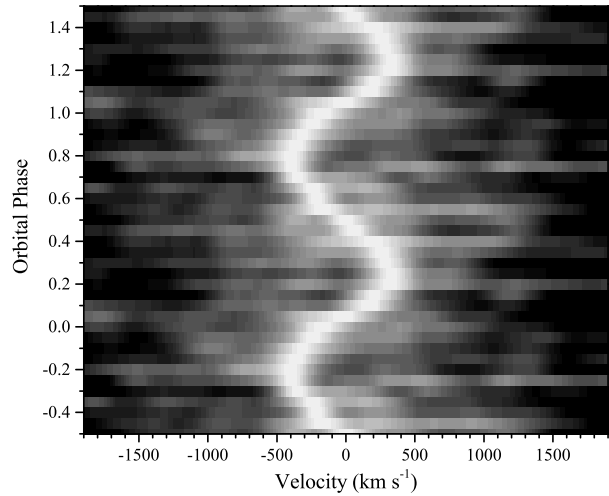


Figure 7. Two-dimensional representation of the cross-correlation function obtained over the wavelength interval of $\lambda\lambda 4350$ – 6510 Å. Two cycles are shown for clarity.

wavelength ranges and they are close to the measurements obtained for the visually detected lines.

In the final step, these solutions were used to create a new cross-correlation template. The cross-correlation analysis was then performed over the full wavelength interval of $\lambda\lambda 4350$ – 6510 Å giving the best-fitting results $K_{2,o} = 382 \pm 8$ km s⁻¹ and the phase zero-point of inferior conjunction of the secondary star ($\phi_0 = 0$) corresponding to $T_0 = \text{HJD } 245\,6510.8081 \pm 0.0005$. In Fig. 6 we show the measured radial velocities together with their sinusoidal fit.

The similarity of the solutions in different wavelength regions leaves no doubts in the reality of the radial velocity variability. The presented analysis also strongly indicates that in addition to the visible spectral lines, there must exist other emission or absorption features in all parts of the spectrum, which are undetectable by eye, but distinguishable by cross-correlation. Using the final cross-correlation template, which essentially is the spectrum of SWIFT J1753.5–0127 corrected for orbital motion of the secondary star, we made another attempt to identify the spectral features of a late-type star, but were again unsuccessful.

A possible reason for our failure may be the extreme conditions under which the donor star existed at the time of our observations. During the outburst stage the secondary should be significantly heated by its companion. Theoretical studies show that a dramatic temperature inversion is expected in the atmosphere of an irradiated M dwarf star. As a result, the emergent spectrum will be significantly different from that of an isolated M dwarf (Barman, Hauschildt, & Allard 2004). Depending on the power of the incident flux and the temperature, pressure, and chemical composition of the secondary’s atmosphere, the resulting spectrum can have complex mixtures of emission and absorption lines. The identification of such a spectrum would be a very complicated task.

3.5 Disc emission lines

We compared the emission lines between the UV and optical data sets and show mean profiles in Fig. 8. In contrast to the UV lines, the optical lines are much weaker (e.g. the peak normalized fluxes of He II $\lambda 1640$ and $\lambda 4686$ are 1.37 and 1.08, respectively), nevertheless their profiles are very similar in shape and width.

The lines are very wide, and the higher excitation lines are much wider than $H\alpha$. This property and the double-peaked appearance of the emission lines suggest their origin in an accretion disc (Smak 1981; Horne & Marsh 1986). Table 3 outlines different parameters of the major emission lines measured from the averaged spectra.

3.5.1 Accretion disc parameters from modelling of the emission line profiles

Despite the similarity of the emission line profiles in SWIFT J1753.5–0127 with those typically observed in other LMXBs, the steepness of the profile wings of high excitation lines (He II and C IV) in SWIFT J1753.5–0127 is quite unusual. It is well known that the shape of the double-peaked profile wings is controlled by the surface radial emissivity profile (Smak 1981; Horne & Marsh 1986). This profile is commonly assumed to follow a power-law model of the form $f(r) \propto r^{-b}$, where r is the radial distance from the compact object. The mechanism powering the emission lines in quiescent accretion discs is discussed in Horne & Saar (1991). Observations of cataclysmic variables (CVs) and BH binaries show that b is usually in range of 1–2, rarely being less than 1.5 (Johnston et al. 1989; Orosz et al. 1994, 2002).

In order to estimate b and other parameters of the accretion disc of SWIFT J1753.5–0127, we fitted the symmetrical double-peaked emission line profiles using a simple model of a uniform flat axisymmetric Keplerian geometrically thin disc (Smak 1981). To calculate the line profiles we used the method of Horne & Marsh (1986). Examples of the application of this technique to the real data are given in Johnston et al. (1989); Orosz et al. (1994, 2002); Neustroev (1998); Neustroev et al. (2002). The three primary free parameters of the model are

- (i) V_{out} , the velocity of the outer rim of the accretion disc;
- (ii) b , the power-law index of the line emissivity profile $f(r)$;
- (iii) $r_{\text{in}}/r_{\text{out}}$, the ratio of the inner to the outer radii of the disc.

Fig. 8 shows four optical and UV emission line profiles together with the corresponding model fits. Parts of the profiles affected by other spectral features (such as deep interstellar absorptions in the centre of C IV and a strong emission feature in the centre of $H\alpha$) were excluded from the fit. The best-fitting model parameters are listed in Table 3 and the errors were estimated with a Monte Carlo approach described in Borisov & Neustroev (1998). The best-fitting power-law index for $H\alpha$ line was $b = 1.58$, which is very close to the values of b found for many other LMXBs. However, the model fits for He II and C IV lines give $b \approx 0$ and even negative values that suggests an unusually flat (or even inverted) radial distribution of the emission-line flux from the accretion disc of SWIFT J1753.5–0127. Because of the lack of data, it is not clear whether such a behaviour is common for BH binaries. However, Marsh & Horne (1990) found that in the dwarf nova IP Peg during an outburst stage, the He II $\lambda 4686$ radial emissivity profile is also remarkably flat compared to the Balmer emission ($b \approx 0.1$ and ≈ 2 , respectively). Marsh & Horne showed that such a behaviour is not in agreement with the predictions of line emission from optically thin discs. They concluded that photoionization by the soft X-rays and UV photons generated in the centre of the accretion disc should be taken into account. We suggest that a similar mechanism may explain the observed properties of the emission lines of SWIFT J1753.5–0127.

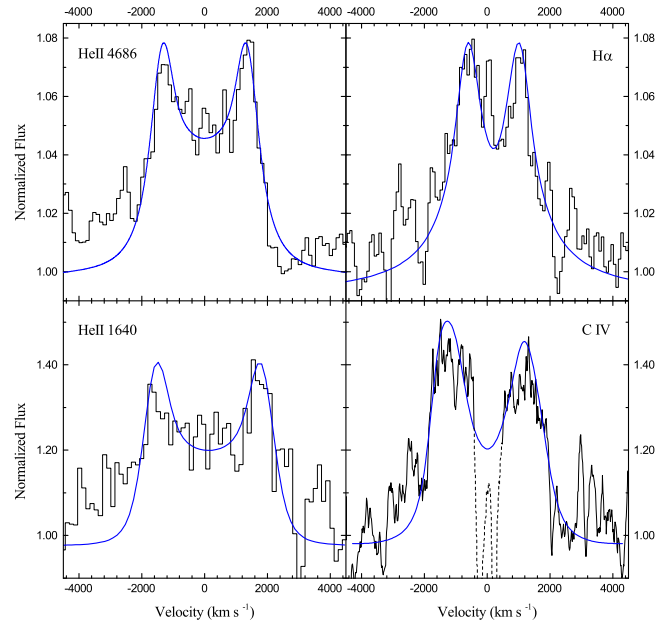


Figure 8. The profiles of the emission lines observed in the optical and UV spectra of SWIFT J1753.5–0127 together with the corresponding model fits.

3.5.2 Orbital variability of the optical emission lines, the equivalent widths and Doppler tomography

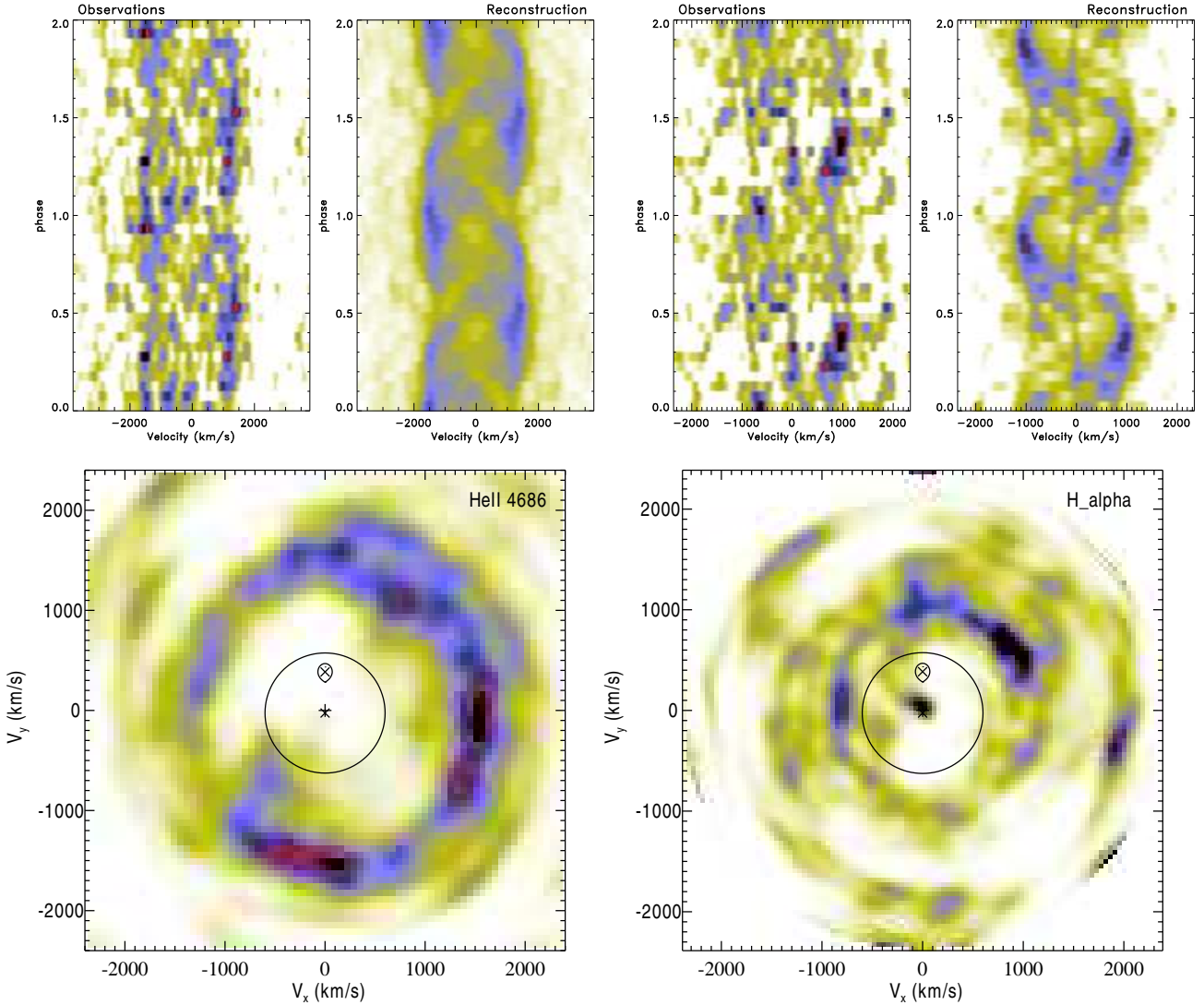
A visual inspection of the optical spectra has shown orbital variations in the line profiles. This is better seen in trailed spectra as variations of the relative intensity of the two peaks in the double-peaked profiles (see top left panels of Fig. 9). We measured the EWs of the emission lines in the phase-folded spectra using the IRAF task *splot* (Fig. 10). The 1σ errors were estimated from the noise fluctuations in the continuum. Though the obtained EWs exhibit rather significant dispersion, none the less we see that they are modulated with the amplitudes of about $\pm 25\%$ of the mean value.

The observed EW minima could be due to an increase in the continuum luminosity when the region of enhanced emission crosses the line-of-sight. There is, however, an apparent shift between the EW curves and optical light curves (see the phase-binned i -band light curve in Fig. 10). The maximum of the optical flux occurs close to the inferior conjunction of the secondary star at phase 0, whereas the EW minima are observed around phase 0.2.

The orbital variation of the emission line profiles indicates the presence of a non-uniform structure in the accretion disc. In order to study it in more detail, we used Doppler tomography. Technical details and examples of the application of Doppler tomography to real data are given by Marsh & Horne (1988) and Marsh (2001). The Doppler maps of the He II $\lambda 4686$ and $H\alpha$ emission lines were computed using the code developed by Spruit (1998). The resulting tomograms are presented in the bottom panels of Fig. 9, whereas the observed and reconstructed emission line profiles are shown in the top panels. To help in interpreting the Doppler maps, additional symbols are inserted, which mark the positions of the compact object (lower cross), the centre of mass of the binary (middle cross) and the Roche lobe of the secondary star (upper bubble with the cross). The circle of radius 600 km s^{-1} around the center of mass corresponds to the projected velocity of the outer part of the largest accretion disc restricted by tidal forces. The Roche lobe of the sec-

Table 3. Parameters of the major emission lines in the averaged spectrum of SWIFT J1753.5–0127.

Spectral line	Flux ($\times 10^{-14}$ erg s $^{-1}$ cm $^{-2}$)	EW (Å)	Relative flux	FWHM (km s $^{-1}$)	Peak-to-peak (km s $^{-1}$)	V_{out} (km s $^{-1}$)	Model parameters b	$r_{\text{in}}/r_{\text{out}}$
H α	0.223	3.6	1.07	2450	1650	798 ± 10	1.58 ± 0.05	0.02 ± 0.01
He II $\lambda 4686$	0.329	4.3	1.08	4200	2690	1370 ± 6	-0.80 ± 0.11	0.06 ± 0.05
He II $\lambda 1640$	1.21	7.1	1.37	4020	3400	1677 ± 7	-0.85 ± 0.11	0.14 ± 0.06
C IV $\lambda 1548.2$	1.33	7.1	1.45	3820	2440	1348 ± 8	0.05 ± 0.12	0.14 ± 0.06
C IV $\lambda 1550.8$						1352 ± 9	0.02 ± 0.15	0.10 ± 0.04

**Figure 9.** Doppler tomography for the He II $\lambda 4686$ and H α emission lines. The top panels show the observed (left) and reconstructed (right) line profiles folded on the orbital period. The corresponding Doppler maps are shown in the bottom panels.

ondary has been plotted using the system parameters: $M_1=3M_\odot$, $M_2=0.2M_\odot$, $i=40^\circ$ (see Section 4).

The observed sharp asymmetric double-peaked profiles of the emission lines produced the azimuthally asymmetric annuli of emission. The radii of the annuli are different for He II and H α , reflecting the different peak-to-peak velocity separation in these lines. However, the overall appearance of the tomograms is rather

similar. They both display the enhanced emission region in the upper-right quadrant. The origin of this structure is unclear. It is located far from the region of interaction between the stream and the disc, which is situated to the left of the secondary star bubble.

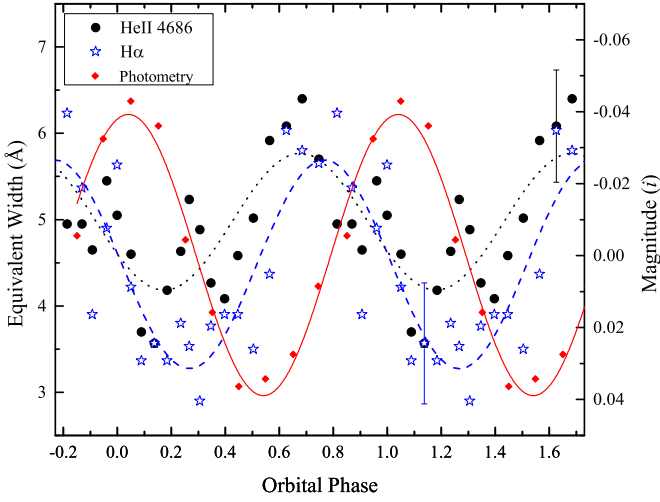


Figure 10. The variation of the EWs of He II 4686 (filled circles) and H α (open stars) with the orbital period. Also shown the phase-binned i -band light curve (red diamonds, the right-hand axis). Two periods are shown for clarity.

The data neither show the emission from the donor which is often observed in the CVs during outbursts².

We also note that the H α data display the low-velocity component which produces a compact spot of emission located around the centre of mass of the binary in the corresponding Doppler map. The source of this feature is not clear. It might be a result of poor subtraction of the geocoronal H α night sky line. However, the phase dependence of this line raise a doubt.

3.5.3 Radial velocity analysis

We attempted to derive the radial velocity curve of the compact object in SWIFT J1753.5–0127 using the double-Gaussian method (Schneider & Young 1980; Shafter 1983), but results were implausible. This is not a surprise, as the method uses the extreme wings of the emission line profile which are very noisy even in the phase-folded spectra of the object because of their steepness. Instead, the radial velocities were measured by fitting the modelled double-peaked profile (see details in Section 3.5.1) to the observed phase-binned profiles. All the primary parameters of the model (V_{out} , b and $r_{\text{in}}/r_{\text{out}}$) were frozen to the averaged values listed in Table 3, but the model profile was allowed to shift along wavelengths. We used only the He II λ 4686 line for this analysis as it has more clear and symmetric profiles than H α and also because it is presumably formed in the inner parts of the accretion disc. Therefore, it should represent the motion of the central star with a higher reliability.

The results are shown in Fig. 11 (right-hand panel). The errors are the formal model fitting errors estimated with a Monte Carlo approach. We made a non-linear least-square fit of the derived velocities to a sinusoid of the form (equation 1), where K_2 was replaced by K_1 . This fit gives the semi-amplitude $K_1 = 52 \pm 10 \text{ km s}^{-1}$, the systemic velocity $\gamma = 6 \pm 6 \text{ km s}^{-1}$ and $\phi_0 = 0.45 \pm 0.03$. The difference between the phase zero-points obtained from the emission and absorption lines is close to 0.5, as expected if the derived velocities from those lines trace the motion of the two compo-

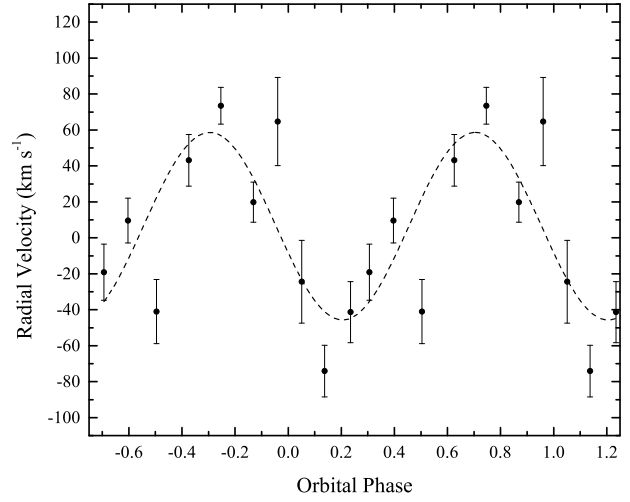


Figure 11. Radial velocities of the He II λ 4686 emission line folded on the ephemeris from Table 4. Two cycles are shown for clarity.

nents. However, it is well known that the parameters obtained with this method are affected by systematic errors, because the emission lines arising from the accretion disc may have severe asymmetric distortions (see, for example, discussion in Orosz et al. 1994). Thus, the obtained value of K_1 should be used with great caution.

4 THE BINARY SYSTEM PARAMETERS

4.1 The K -correction

The observed values of $K_{2,o}$ are often known to suffer from non-uniform distribution of absorption or emission spectral features on the donor star surface due to the heating effect by irradiation from the X-ray source. The noncoincidence of the centre-of-mass and the centre-of-light of the donor can result in systematic errors in the determined velocity amplitude $K_{2,o}$. A mixture of emission and absorption lines in the spectrum of SWIFT J1753.5–0127 strongly suggests that irradiation of the secondary plays a significant role. Moreover, the flux at 5000 Å from a low-mass star with temperature of 3000 K and radius of $2 \times 10^{10} \text{ cm}$ at 2 kpc is expected to be considerably smaller than the observed one ($F_\lambda \approx 2.5 \times 10^{-19}$ and $7 \times 10^{-16} \text{ erg s}^{-1} \text{ cm}^{-2} \text{ Å}^{-1}$, respectively). Thus, no lines from the dark side of the star should be visible in the observed spectrum. This suggests that the cross-correlation signal likely originates in the irradiated surface of the secondary. Therefore, in order to obtain the true value of K_2 , a ‘ K -correction’ should be applied.

The K -correction generally depends on the mass ratio and the distribution of spectral line emission or absorption over the surface of the secondary star and can be expressed as (Wade & Horne 1988; see also equation 2.77 in Warner 1995):

$$\frac{K_{2,o}}{K_2} \approx 1 - 0.462q^{1/3}(1+q)^{2/3} \frac{\Delta R_2}{R_2}, \quad (2)$$

where q is the mass ratio M_2/M_1 , R_2 is the radius of the secondary and ΔR_2 is the displacement of the centre-of-light from the centre of mass of the secondary star. It is difficult to quantify the correction without the knowledge of these parameters. In order to estimate its reliable extreme value, we adopted the realistic values of $q = 0.04 - 0.12$ (see Section 4.5) and assumed $\Delta R_2/R_2$ to be ~ 0.5 that roughly corresponds to the extreme case where the

² However, a bright compact spot at the position of the secondary star is clearly seen in a Doppler map of the emission line at λ 5193 Å.

spectral lines come only from the hemisphere closest to the primary. Within these assumptions $K_{2,o}/K_2$ is in the range 0.88–0.92, therefore in the following analysis we use $K_{2,o}/K_2 = 0.9$ as an illustration for a possible K -correction.

In theory, the correction can be larger if emission is tightly concentrated near the L_1 -point. However, this is not supported by observations. Such a compact emission source should be luminous enough to produce a visible structure in the $H\alpha$ Doppler map. Moreover, in a realistic situation, the accretion disc’s outer rim casts a broad shadow on to the donor star, and only relatively small areas near the poles of the donor’s facing hemisphere can be directly irradiated by the central X-ray source. In order for the secondary star to be illuminated, indirect irradiation via scattered X-rays should be taken into account, or there should exist another source of irradiation, located outside the equatorial plane. Both these scenarios imply that sufficiently extended regions on the donor star will be irradiated (for a detailed discussion, see Dubus et al. 1999; Ritter 2008).

4.2 Mass function and constraints on the compact object mass from the double-peaked emission lines

The semi-amplitude K_2 of the secondary’s radial velocity curve and the orbital period P_{orb} give the mass function which sets an absolute lower limit for the mass of the compact object:

$$f(M) = \frac{K_2^3 P_{\text{orb}}}{2\pi G} = \frac{M_1^3 \sin^3 i}{(M_1 + M_2)^2}, \quad (3)$$

where M_1 is the mass of the compact object, M_2 is the mass of the secondary star and i is the binary inclination. From the observed velocity $K_{2,o} = 382 \text{ km s}^{-1}$ we can calculate the “observed” mass function $f_o(M) = 0.69 \pm 0.04 M_\odot$. Applying the K -correction, we obtain the mass function $f(M) \lesssim 0.95 M_\odot$, which is one of the smallest mass function for a BH LMXB (Casares & Jonker 2014).

Another independent approach to constrain the compact object mass is to measure the outer disc velocity. Smak (1981) has shown that assuming the Keplerian velocity in the accretion disc

$$V_K = \sqrt{\frac{GM_1}{r}}, \quad (4)$$

the double-peaked profiles can be used to determine the projected velocity V_{out} of the outer rim of the accretion disc, which, in turn, depends on the mass M_1 of the accreting star and the radius of the disc. The largest radius of the accretion disc, should it be determined from observations, can further constrain the system parameters.

We measured $V_{\text{out}} \approx 800 \text{ km s}^{-1}$ through the modelling of the $H\alpha$ emission line, which originates in the outermost part of the accretion disc (see Section 3.5.1 and Table 3). We note, however, that during our observations both $H\alpha$ and $\text{He II } \lambda 4686$ lines were much wider than they were at the beginning of the outburst, when the peak-to-peak separation for $H\alpha$ was 1200–1300 km s^{-1} (Torres et al. 2005).

This implies that the accretion disc of SWIFT J1753.5–0127 has shrunk by about 45 per cent compared to the early phase of the outburst, similar to what was observed in other LMXBs (Calvelo et al. 2009) and in CVs (Warner 1995). In this context we note that the outer parts of a large accretion disc are under the gravitational influence of the secondary star, which prevents the disc from growing above the tidal truncation radius r_{max} , where the tidal and viscous stresses are comparable (Warner 1995 and references therein). It can be estimated as (see equation 2.61 in Warner 1995):

$$r_{\text{max}} = a \frac{0.6}{1+q}, \quad (5)$$

where a is the binary separation. Combining Kepler’s third law with equations (4) and (5), we obtain the relation:

$$(M_1 + M_2) \sin^3 i = \frac{0.074 P_{\text{orb}} V_{K,\text{max}}^3}{G}, \quad (6)$$

where $V_{K,\text{max}}$ is the projected Keplerian velocity of the accretion disc at the tidal radius. Adopting Torres et al.’s value for V_{out} of 600 km s^{-1} as an estimate of $V_{K,\text{max}}$ we get $(M_1 + M_2) \sin^3 i = 1.2 M_\odot$. Using the realistic value of $0.2 M_\odot$ for the secondary mass (see Section 4.3), we find that the solutions for M_1 for any inclination are in good agreement with the solutions obtained from the mass function with the K -correction applied (Fig. 12).

4.3 Constraints on the secondary mass

It is clear that the secondary is a low-mass star, otherwise its absorption lines would be much more apparent in the spectrum of SWIFT J1753.5–0127. In order to be transferring matter on to the compact component, the secondary star must fill its Roche lobe. The relative size of the donor star is therefore constrained by the Roche geometry and the donor must obey the period-density relation for the Roche lobe filling objects (Warner 1995). If the secondary is a main-sequence star, one immediately gets an estimate for the mass. The empirical and theoretical mass-period relations for a 2.85 h orbital period binary yield the mass of the secondary star in the range 0.17 – $0.25 M_\odot$ (Warner 1995; Smith & Dhillon 1998; Patterson et al. 2005). If the donor is an evolved star, it is likely somewhat inflated relative to isolated main-sequence stars of the same mass, thus the mass inferred from such relation can be considered as an upper limit (Kolb et al. 2001; Knigge 2012). The recently calculated evolutionary sequences for NS binaries with a 3 h period obtain the secondary masses in the range 0.1 – $0.3 M_\odot$ (Podsiadlowski et al. 2002; Lin et al. 2011). We conservatively assume this mass range for the secondary in SWIFT J1753.5–0127.

4.4 Constraints on the inclination

It is clear from the discussion above that the companion mass is rather low, and therefore the BH mass mostly depends on the unknown inclination of the system and the possible K -correction. Even though the BH mass can be rather large for small i , there are additional observational reasons which argue against a very low orbital inclination angle.

(i) The UV spectrum of SWIFT J1753.5–0127 is dominated by relatively strong emission lines C IV and He II without P Cyg absorption components, and no other absorption lines are detected. From studies of CVs with high accretion mass rates (nova-like stars and dwarf novae in outbursts) it is known that the appearance of their UV spectra strongly depends on orbital inclination: low inclination systems show mainly absorption features in spectra, intermediate-to-low inclination systems exhibit P Cyg profiles and/or blue-shifted deep absorptions, whereas high inclination systems show strong emission lines (La Dous 1989; Puebla et al. 2007, 2011). It is not clear if these results can be applied to LMXBs whose accretion discs are strongly irradiated by the X-rays from the inner region. Published UV spectra of LMXBs show relatively strong emission lines. However, to the best of our knowledge, no UV observations of any low or intermediate-to-low inclination systems are available in the literature. Thus, based on the results of the

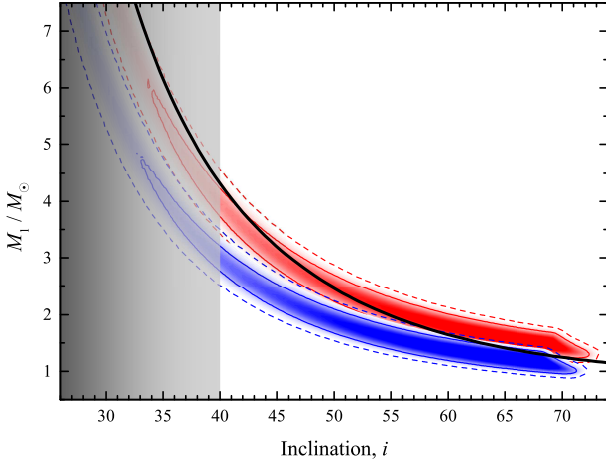


Figure 12. Constraints on the black hole mass M_1 in SWIFT J1753.5–0127 obtained using a Monte Carlo simulation of the observed parameters. The blue area corresponds to the observed semi-amplitude $K_{2,o}$, whereas the red data are calculated for the K -correction $K_{2,o}/K_2 = 0.9$. Denser colours represent higher probability. The solid and dashed lines are the 68 per cent and 95 per cent confidence levels, respectively. The black line shows the BH mass as set by the relation (6) for $M_2 = 0.2M_\odot$. The shaded area marks the improbable solutions because of the observed strong photometric and spectroscopic orbital variability (see the text for explanation).

numerical simulations of CVs (La Dous 1989; Puebla et al. 2011), we can put a lower limit of $i \gtrsim 40^\circ$.

(ii) The time resolution optical light curves of SWIFT J1753.5–0127 obtained during our observations display prominent orbital variations with the amplitude of 0.10–0.15 mag in V (Fig. 3), whose nature is not yet clear. The source of orbital modulation cannot be the varying aspect of the irradiated secondary star because the maximum of light is observed around phase 0.0, i.e. inferior conjunction of the secondary star. This also can hardly be a bright spot or bulge on the outer edge of the disc formed by the impact of the gas stream. SWIFT J1753.5–0127 is still in outburst, thus its accretion disc is in the hot, ionized state. The observations of CVs and LMXBs show that the bright spot is barely seen during the outburst stage. Most likely, this orbital modulation is due to some substructures in the non-uniform or/and non-axisymmetric accretion disc (i.e. spiral waves, warps or tidally thickened regions). The detection of the enhanced emission regions in the Doppler maps and of the EW variability supports this idea. It is quite obvious that a low-inclination binary system is unable to produce a relatively large amplitude EW variability and orbital modulation in the light curve. Our simulations have shown (see Appendix A) that for more or less realistic parameters of the bright area in the accretion disc it is virtually impossible to obtain the orbital variability with the required amplitude for the orbital inclination $i \lesssim 40^\circ$.

On the other hand, large inclinations are ruled out too, because both ours and the published photometry and spectroscopy of SWIFT J1753.5–0127 are extensive enough to rule out any significant eclipse. The maximal possible inclination in absence of eclipses generally depends on the mass ratio and can be estimated as

$$\cos i \gtrsim \frac{R_2/a}{1 - r_d/a}, \quad (7)$$

Table 4. Orbital and system parameters for SWIFT J1753.5–0127.

Parameter	Value
Observed	
P_{orb} (h)	2.85 ± 0.01
T_0 (+2450000)	6510.8081 ± 0.0005
K_1 (km s $^{-1}$)	52 ± 10
$K_{2,o}$ (km s $^{-1}$)	382 ± 8
γ (km s $^{-1}$)	6 ± 6
$f_o(M)/M_\odot$	0.69 ± 0.04
Constrained	
i	$\gtrsim 40^\circ$
M_1/M_\odot	$\lesssim 3.1$ (4.1) ^a
M_2/M_\odot	0.1–0.3
$q = M_2/M_1$	$\gtrsim 0.04$ (0.03)
a/R_\odot	$\lesssim 1.53$ (1.67)

^aThe numbers in parentheses correspond to the solutions with the K -correction applied.

where r_d is the disc size, which we assume to be equal to 60 per cent of the maximal tidally-allowed size r_{max} (see Section 4.2), and the nominator is computed from the Eggleton (1983) formula:

$$\frac{R_2}{a} = \frac{0.49q^{2/3}}{0.6q^{2/3} + \ln(1 + q^{1/3})}. \quad (8)$$

4.5 Observational and Monte-Carlo constraints on the binary system parameters

From the above analysis we can put a conservative lower limit for the orbital inclination to be $i \gtrsim 40^\circ$, constrain its upper limit using Equation (7), and consequently restrict the BH mass M_1 to the ranges 1.0–3.1 M_\odot for the observed $K_{2,o}$ and 1.3–4.1 M_\odot with the K -correction applied.

In order to illustrate the cumulative effect of uncertainty in input parameters, we also applied a Monte-Carlo approach using 10^8 trials for Gaussian distribution of K_2 (with $\sigma = 8$ km s $^{-1}$), a top-hat distribution of secondary mass in the limits of 0.1–0.3 M_\odot and a uniform distribution of $\cos i$. The simulations were performed for the observed $K_{2,o}$ and with the K -correction applied ($K_2 = K_{2,o}/0.9$). For any set $(M_2, i, K_{2,o})$ we calculate M_1 from the mass function, and the parameters are accepted if there are no eclipses (equation 7).

Fig. 12 shows the results of the Monte-Carlo simulations with the formal 68 and 95 per cent confidence levels³. Denser colours represent higher probability reflecting a strong tendency for lower masses. In the figure we also show the BH mass as set by the relation (6) based on constraints obtained from the double-peaked emission lines. These calculations show that the compact object mass in excess of 5 M_\odot is rather improbable, because it requires an extremely large K -correction or a lower inclination angle, which is also unlikely because of the observed strong photometric and spectroscopic orbital variability.

We note that even with the lowest possible upper limit on the inclination and the large K -correction, the solution allows for the

³ The simulations were performed without additional limitations which should be applied but which values are not well defined (e.g., the minimal orbital inclination). This biases the Monte-Carlo tests and may affect the confidence levels.

compact object mass to be below $1.3 M_{\odot}$, that would correspond to a low-mass NS. Nevertheless, X-ray properties of SWIFT J1753.5–0127 are typical for a BH binary and argue strongly in favour of a BH accretor in the system. This fact can be used to impose an additional restriction on the solution by requiring that the BH has a mass greater than some specified limit, e.g. the maximum possible NS mass. Following the modern theoretical calculations, which give the maximum NS mass $\lesssim 2.4 M_{\odot}$ (Lattimer 2012), this limit can be put at $2.5 M_{\odot}$. Nevertheless, admitting that the value of this limit is not well defined, we leave this discussion for the interested reader to complete.

The values of the measured and constrained system parameters are summarised in Table 4. In Fig. 13 we show a schematic representation of the suggested geometry for SWIFT J1753.5–0127, plotted using the system parameters: $M_1=3 M_{\odot}$, $M_2=0.2 M_{\odot}$, $i=40^\circ$.

The presented BH mass calculations were done with the orbital period of 2.85 h. However, even if the previous value ~ 3.2 h found by Zurita et al. (2008) appears to be the correct orbital period, the results will not change significantly due to the relatively weak dependence of the mass function on the period and a large uncertainty in other parameters.

5 DISCUSSION

5.1 The BH mass

According to the current convention, the black holes are compact objects, whose measured masses exceed the limit of $3 M_{\odot}$. To date, many BH binaries were identified according to the high measured mass function $f(M) > 3 M_{\odot}$, which puts an absolute lower limit for the primary mass (Casares & Jonker 2014). In a number of other systems, additional constraints were required to obtain the mass of the compact object in excess of this limit. The inferred masses of BHs used to be well above the value $3 M_{\odot}$, while the measured NS masses tend to cluster at ~ 1.4 – $1.5 M_{\odot}$ (Remillard & McClintock 2006; Lattimer 2012). The observed distribution of compact objects thus seems to have a double-peak structure at $\sim 1.5 M_{\odot}$ and $\sim 7 M_{\odot}$ for NSs and BHs, correspondingly (Bailyn et al. 1998; Özel et al. 2010), with a gap in the mass range 2 – $5 M_{\odot}$. Investigations of the minimal possible black hole mass (Farr et al. 2011) gave $M_{\text{BH,min}} \sim 4.3 M_{\odot}$, significantly above the maximum NS mass, further supporting the existence of a gap. Theoretical interpretation of the observed mass distribution was given in the context of different supernova mechanisms (Belczynski et al. 2012): the gap appeared in the simulations with rapidly developing explosions (launched within ~ 0.2 s after the core bounce), while the delayed explosions (developing on timescales ~ 0.5 – 1 s) result in continuous mass distribution. The obtained range of masses for SWIFT J1753.5–0127 put the binary right into the 2 – $5 M_{\odot}$ gap, suggesting that the object might be formed in the delayed explosion scenario. Alternatively, the primary mass, initially below $2 M_{\odot}$, could have been enhanced as a result of the accretion processes on the Hubble timescale, to reach the maximum possible mass of a stable NS and then collapsed into a BH. Such effects of binary evolution were considered in Belczynski et al. (2012), who showed that this results in the small additional number of objects with the masses in the range 2 – $3 M_{\odot}$.

On the other hand, investigations of Kreidberg et al. (2012) suggest that the gap is an artefact of systematic uncertainties in mass measurements. They conclude that the BH masses in two objects, GRO J0422+32 and 4U 1543–47, plausibly lie within the

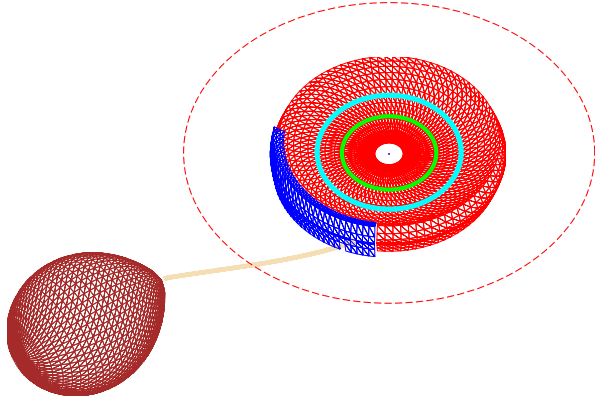


Figure 13. A schematic representation of the suggested geometry for SWIFT J1753.5–0127 plotted using the system parameters: $M_1=3M_{\odot}$, $M_2=0.2M_{\odot}$, $i=40^\circ$. The red thick dashed circle shows the largest radius of the accretion disc determined by tidal limitations. We suggest that it was the accretion disc outer radius during the observations of Torres et al. (2005). At the time of our optical observations the disc (shown as a red disc) has shrunk by about 45 per cent compared to Torres et al.’s observations. The cyan and green rings represent the disc outer radii in which emission lines with higher excitation energies than $H\alpha$ were originated at the time of observations (cyan: He II $\lambda 4686$ and C IV, green: He II $\lambda 1640$). The blue segment located at the outer rim of the accretion disc in front of the secondary shows the bright area which position is assigned according to the relative phasing of the photometric and radial velocity modulations.

mass gap. Other ‘outliers’ include the binary 4U 1700–37, $M = 2.44 \pm 0.27 M_{\odot}$ (Clark et al. 2002), for a long time being classified as a NS (Reynolds et al. 1999), but again returning to the originally proposed (e.g. Brown et al. 1996) BH class by the discovery of the very low-frequency QPOs (Dolan 2011). The compact object in the classical BH candidate Cyg X-3 was recently estimated to have $M = 2.4^{+2.1}_{-1.1} M_{\odot}$ (Zdziarski et al. 2013), again right in the middle of the mass gap. Our estimates for SWIFT J1753.5–0127 further support the existence of compact objects with masses in the range 2 – $5 M_{\odot}$. A re-analysis of the full set of data is probably required to conclude whether the mass gap still exists.

Masses of BHs used to be comfortably above the limit of $3 M_{\odot}$. However, a growing amount of measurements suggest that there exist a population of compact objects very close to this limit. They can be formed either in the processes of the delayed supernova explosion (such as in simulations of Belczynski et al. 2012) or by the accretion-induced collapse of the NS (initially formed in the supernova explosion) during the common-envelope phase or by accretion from the companion on the Hubble time. It becomes evident that the firm classification based on the compact object mass estimate alone is becoming less and less reliable, and other diagnostic method should be agreed on to serve a criterion to distinguish between BHs and NSs. Such a technique will likely be based on the difference of observational appearance of objects with and without solid surface. The most promising methods are based on the X-ray colour evolution as a function of flux (Done & Gierliński 2003) and on the properties of the broad-band noise (Sunyaev & Revnivtsev 2000).

5.2 Orbital period

Both our photometric and spectroscopic data suggest the orbital period of SWIFT J1753.5–0127 2.85 h. This puts the system right into

the so-called period gap between about 2.15 and 3.18 h (according to results of Knigge 2006). The gap marks the dearth of active CVs in this period range, which appear to have smaller radii compared to the Roche lobe size. The traditional explanation of the period gap involves a thermal bloating of the secondary at periods above ~ 3 h due to enhanced mass transfer rates (due to magnetic braking mechanism) over those driven by the gravitational radiation losses alone (Howell et al. 2001; Knigge et al. 2011). The magnetic braking abruptly stops at this upper limit when the secondary becomes fully convective (Spruit & Ritter 1983), leading to a reduction of the mass-loss rate and, as a result, its contraction. The binary continues to evolve towards shorter periods as detached system, and eventually the Roche lobe becomes small enough to resume the mass transfer. The fact that SWIFT J1753.5–0127 displays an outburst whilst having the period in the middle of the gap supports our suggestion that the secondary is a slightly evolved star, whose radius is larger than that of a main-sequence star of the same mass. The same conclusion was reached for the LMXB MAXI J1659–152 (2.4 h, Kuulkers et al. 2013) and can also be applied to SWIFT J1357.2–0933 (2.8 h, Corral-Santana et al. 2013).

6 SUMMARY

Despite of the long history of study, system parameters of SWIFT J1753.5–0127 apart from the orbital period were not investigated. The system exhibits X-ray properties typical for the BH binary and has always been considered in the context of the BH primary. Its mass, however, was not dynamically measured, and the assumed values in some cases reached $12 M_{\odot}$ (Zurita et al. 2008; Froning et al. 2014). For the first time, we performed the analysis of spectroscopic data to determine the system parameters. Our main result is that the primary in SWIFT J1753.5–0127 is not at all so massive – its mass in excess of $5 M_{\odot}$ is highly improbable. This result not only affects the modelling of spectral properties, but also supports the possibility of existence of compact objects in the range 2–5 M_{\odot} , the so-called mass gap. The later conclusion greatly limits the formation scenarios. For instance, in the rapid supernova explosion mechanisms, it is not possible to produce the compact objects with masses 3–5 M_{\odot} , even accounting for the binary evolution effects. We suggest that the primary in SWIFT J1753.5–0127 can either be produced in the delayed explosion or be the result of the accretion-induced collapse of a NS.

We also performed time series analysis of our photometric and spectroscopic data and confirm that SWIFT J1753.5–0127 is one of the shortest period X-ray binaries, as initially proposed by Zurita et al. (2008). Our data, however, are better described by the orbital period of 2.85 h, in contrast to ~ 3.24 h found by them. This finding puts the system into the well-known period gap, in which the main-sequence companions do not fill their Roche lobes. The fact that SWIFT J1753.5–0127 is still in outburst suggests that the mass transfer proceeds, therefore, the companion has a radius larger than that of a main sequence star of the same mass. This is naturally explained if the secondary is somewhat nucleary evolved.

ACKNOWLEDGMENTS

This work was supported by the Finnish Doctoral Program in Astronomy and Space Physics (AV) and the Academy of Finland grant 268740 (JP). SZ acknowledges PAPIIT grants IN-100614 and CONACyT grants 151858 and CAR 208512 for resources provided

toward this research. JJEK acknowledges partial financial support from the Emil Aaltonen Foundation and the Väisälä Foundation. Our research was partially based on UV observations by NASA missions *HST* and *Swift* which we acknowledge. We thank Neil Gehrels for approving the Target of Opportunity observation with *Swift* and the *Swift* team for executing the observation. This research has made use of data obtained through the High Energy Astrophysics Science Archive Research Center Online Service, provided by the NASA/Goddard Space Flight Center. We would like to acknowledge the anonymous referee whose comments have significantly improved this paper.

REFERENCES

- Bailyn C. D., Jain R. K., Coppi P., Orosz J. A., 1998, *ApJ*, 499, 367
- Barman T. S., Hauschildt P. H., Allard F., 2004, *ApJ*, 614, 338
- Barret D., Olive J. F., Boirin L., Done C., Skinner G. K., Grindlay J. E., 2000, *ApJ*, 533, 329
- Belczynski K., Wiktorowicz G., Fryer C. L., Holz D. E., Kalogera V., 2012, *ApJ*, 757, 91
- Belloni T. M., Motta S. E., Muñoz-Darias T., 2011, *Bull. Astr. Soc. India*, 39, 409
- Berry R., Burnell J., 2005, *The handbook of astronomical image processing*, 2nd ed. Willmann-Bell, Richmond, VA
- Borisov N. V., Neustroev V. V., 1998, *Bull. Spec. Astrophys. Obs.*, 44, 110 (astro-ph/9806159)
- Brown G. E., Weingartner J. C., Wijers R. A. M. J., 1996, *ApJ*, 463, 297
- Butler N. et al., 2012, *SPIE*, 844610
- Cadotte Bel M. et al., 2007, *ApJ*, 659, 549
- Calvelo D. E., Vrilek S. D., Steeghs D., Torres M. A. P., Neilsen J., Filippenko A. V., González Hernández J. I., 2009, *MNRAS*, 399, 539
- Casares J., Jonker P. G., 2014, *SSRv*, 183, 223
- Casares J., Steeghs D., Hynes R. I., Charles P. A., O’Brien K., 2003, *ApJ*, 590, 1041
- Chiang C. Y., Done C., Still M., Godet O., 2010, *MNRAS*, 403, 1102
- Clark J. S., Goodwin S. P., Crowther P. A., Kaper L., Fairbairn M., Langer N., Brocksopp C., 2002, *A&A*, 392, 909
- Corral-Santana J. M., Casares J., Muñoz-Darias T., Rodríguez-Gil P., Shahbaz T., Torres M. A. P., Zurita C., Tyndall A. A., 2013, *Sci*, 339, 1048
- Dolan J. F., 2011, arXiv:1107.1537
- Done C., Gierliński M., 2003, *MNRAS*, 342, 1041
- Dubus G., Lasota J.-P., Hameury J.-M., Charles P., 1999, *MNRAS*, 303, 139
- Durant M., Gandhi P., Shahbaz T., Peralta H. H., Dhillon V. S., 2009, *MNRAS*, 392, 309
- Eggleton P. P., 1983, *ApJ*, 268, 368
- Farr W. M., Sravan N., Cantrell A., Kreidberg L., Bailyn C. D., Mandel I., Kalogera V., 2011, *ApJ*, 741, 103
- Froning C. S., Maccarone T. J., France K., Winter L., Robinson E. L., Hynes R. I., Lewis F., 2014, *ApJ*, 780, 48
- Gehrels N. et al., 2004, *ApJ*, 611, 1005
- Gierliński M., Poutanen J., 2005, *MNRAS*, 359, 1261
- Gilfanov M., 2010, in *Lecture Notes in Physics*, Vol. 794, *The Jet Paradigm*, T. Belloni, ed., Springer-Verlag, Berlin, pp. 17–52
- Horne K., Marsh T. R., 1986, *MNRAS*, 218, 761
- Horne K., Saar S. H., 1991, *ApJL*, 374, L55

- Howell S. B., Nelson L. A., Rappaport S., 2001, *ApJ*, 550, 897
- Hynes R. I., Steeghs D., Casares J., Charles P. A., O’Brien K., 2003, *ApJL*, 583, L95
- Ibragimov A., Poutanen J., 2009, *MNRAS*, 400, 492
- Johnston H. M., Kulkarni S. R., Oke J. B., 1989, *ApJ*, 345, 492
- Knigge C., 2006, *MNRAS*, 373, 484
- Knigge C., 2012, *MmSAI*, 83, 549
- Knigge C., Baraffe I., Patterson J., 2011, *ApJS*, 194, 28
- Kolb U., King A. R., Baraffe I., 2001, *MNRAS*, 321, 544
- Kreidberg L., Bailyn C. D., Farr W. M., Kalogera V., 2012, *ApJ*, 757, 36
- Kuulkers E. et al., 2013, *A&A*, 552, A32
- La Dous C., 1989, *A&A*, 211, 131
- Lattimer J. M., 2012, *ARNPS*, 62, 485
- Lin D., Remillard R. A., Homan J., 2007, *ApJ*, 667, 1073
- Lin D., Remillard R. A., Homan J., 2010, *ApJ*, 719, 1350
- Lin J., Rappaport S., Podsiadlowski P., Nelson L., Paxton B., Todorov P., 2011, *ApJ*, 732, 70
- Marsh T. R., 2001, in *Astromotography, Indirect Imaging Methods in Observational Astronomy*, ed. H. M. J. Boffin, D. Steeghs, and J. Cuypers, *Lect. Notes Phys.*, 573, 1
- Marsh T. R., Horne K., 1988, *MNRAS*, 235, 269
- Marsh T. R., Horne K., 1990, *ApJ*, 349, 593
- Massa D., Aloisi A., Keyes C., Bohlin R., Froning C., 2010, *Instrument Science Report COS 2010-01(v1)*. Space Telescope Science Institute
- Morgan E., Swank J., Markwardt C., Gehrels N., 2005, *ATel*, 550, 1
- Muñoz-Darias T., Casares J., Martínez-Pais I. G., 2008, *MNRAS*, 385, 2205
- Neustroev V. V., 1998, *Astr. Rep.*, 42, 748
- Neustroev V. V., Borisov N. V., Barwig H., Bobinger A., Mantel K. H., Šimić D., Wolf S., 2002, *A&A*, 393, 239
- Neustroev V. V., Zharikov S., 2008, *MNRAS*, 386, 1366
- Oke J. B., 1990, *AJ*, 99, 1621
- Orosz J. A., Bailyn C. D., Remillard R. A., McClintock J. E., Foltz C. B., 1994, *ApJ*, 436, 848
- Orosz J. A. et al., 2002, *ApJ*, 568, 845
- Özel F., Psaltis D., Narayan R., McClintock J. E., 2010, *ApJ*, 725, 1918
- Palmer D. M., Barthelmey S. D., Cummings J. R., Gehrels N., Krimm H. A., Markwardt C. B., Sakamoto T., Tueller J., 2005, *ATel*, 546, 1
- Patterson J. et al., 2005, *PASP*, 117, 1204
- Podsiadlowski P., Rappaport S., Pfahl E. D., 2002, *ApJ*, 565, 1107
- Poole T. S. et al., 2008, *MNRAS*, 383, 627
- Poutanen J., Gierliński M., 2003, *MNRAS*, 343, 1301
- Puebla R. E., Diaz M. P., Hillier D. J., Hubeny I., 2011, *ApJ*, 736, 17
- Puebla R. E., Diaz M. P., Hubeny I., 2007, *AJ*, 134, 1923
- Remillard R. A., McClintock J. E., 2006, *ARA&A*, 44, 49
- Reynolds A. P., Owens A., Kaper L., Parmar A. N., Segreto A., 1999, *A&A*, 349, 873
- Ritter H., 2008, *NewAR*, 51, 869
- Schneider D. P., Young P., 1980, *ApJ*, 238, 946
- Shafter A. W., 1983, *ApJ*, 267, 222
- Smak J., 1981, *AcA*, 31, 395
- Smith D. A., Dhillon V. S., 1998, *MNRAS*, 301, 767
- Soleri P. et al., 2013, *MNRAS*, 429, 1244
- Soria R., Wu K., Johnston H. M., 1999, *MNRAS*, 310, 71
- Spruit H. C., 1998, preprint (astro-ph/9806141)
- Spruit H. C., Ritter H., 1983, *A&A*, 124, 267
- Steeghs D., Casares J., 2002, *ApJ*, 568, 273
- Sunyaev R., Revnivtsev M., 2000, *A&A*, 358, 617
- Torres M. A. P. et al., 2005, *ATel*, 566, 1
- Tovmassian G., Stephania Hernandez M., González-Buitrago D., Zharikov S., García-Díaz M. T., 2014, *AJ*, 147, 68
- Wade R. A., Horne K., 1988, *ApJ*, 324, 411
- Warner B., 1995, *Cataclysmic variable stars*, Cambridge Astrophysics Series, No. 28. Cambridge University Press, Cambridge
- Watson A. M. et al., 2012, *SPIE*, 84445L
- Zdziarski A. A., Gierliński M., 2004, *Prog. Theor. Phys. Suppl.*, 155, 99
- Zdziarski A. A., Mikolajewska J., Belczyński K., 2013, *MNRAS*, 429, L104
- Zdziarski A. A., Poutanen J., Mikolajewska J., Gierliński M., Ebisawa K., Johnson W. N., 1998, *MNRAS*, 301, 435
- Zharikov S., Tovmassian G., Aviles A., Michel R., Gonzalez-Buitrago D., García-Díaz M. T., 2013, *A&A*, 549, A77
- Zurita C., Durant M., Torres M. A. P., Shahbaz T., Casares J., Steeghs D., 2008, *ApJ*, 681, 1458

APPENDIX A: BRIEF DESCRIPTION OF THE LIGHT-CURVE SIMULATIONS

The detailed fitting of the light curve of SWIFT J1753.5–0127 requires to make certain assumptions on the accretion disc structure which we do not know. In order to reproduce the observed light curve of SWIFT J1753.5–0127 in terms of shape and amplitude, we adopted the modelling technique from Zharikov et al. (2013) and Tovmassian et al. (2014). A simple geometrical model of SWIFT J1753.5–0127, presented in Fig. 13 is comprised of a concave accretion disc, a secondary red dwarf star, a stream from the inner Lagrangian point, and a bright area located at the outer rim of the accretion disc in front of the secondary.

We assume that the steady-state, optically thick, viscous accretion disc radiates as a blackbody at the local temperature which radial distribution across the disc is given by $T(r) = T_{\text{out}}(r/r_{\text{out}})^{-3/4}$, where T_{out} is the temperature at the outer edge of the disc. The bright area is characterized by the azimuthal extension θ and the temperature T_b . The vertical extension of the bright area is equal to the thickness of the concave accretion disc at the outer edge and characterized by the opening angle z as seen from the BH. The donor star fills its Roche lobe. Emission from the accretion stream is not taken into account. The surface of each component of the system is divided in a series of triangles as shown in Fig. 13, each triangle emits as a blackbody with corresponding temperature. The total flux from the binary is obtained by integrating the emission from all the elements lying in a sight of view and then folded with the response of the V filter.

The fixed parameters for the model are set as follows:

- (i) The mass of the primary is $3M_{\odot}$;
- (ii) the mass of the donor star is $0.2M_{\odot}$;
- (iii) the temperature of the donor star is 3000K;
- (iv) the outer and inner radii of the disc are imposed by the parameters $V_{\text{out}} = 800 \text{ km s}^{-1}$ and $r_{\text{in}}/r_{\text{out}} = 0.02$ estimated for the $H\alpha$ emission line (see Section 3.5.1 and Table 3);
- (v) the temperature at the outer edge of the disc is $T_{\text{out}}=8000\text{K}$.

We calculated a variety of models using different bright area parameters. We found that the shape of the light curve mostly depends on the azimuthal extension θ whereas the amplitude of variability relies on the orbital inclination i , the opening angle of the

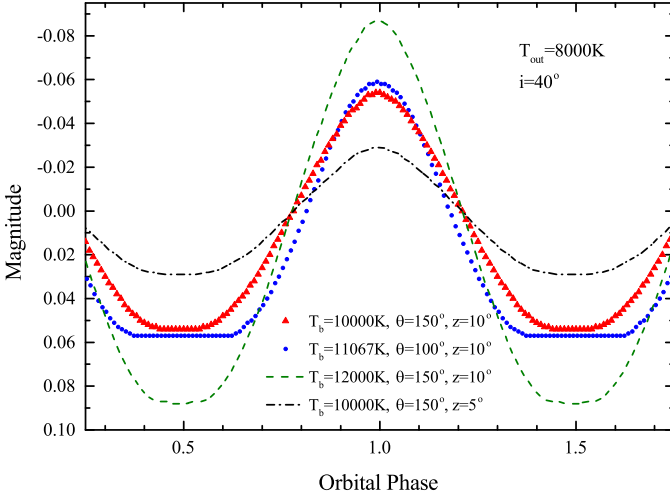


Figure A1. Light curves calculated for different bright area parameters.

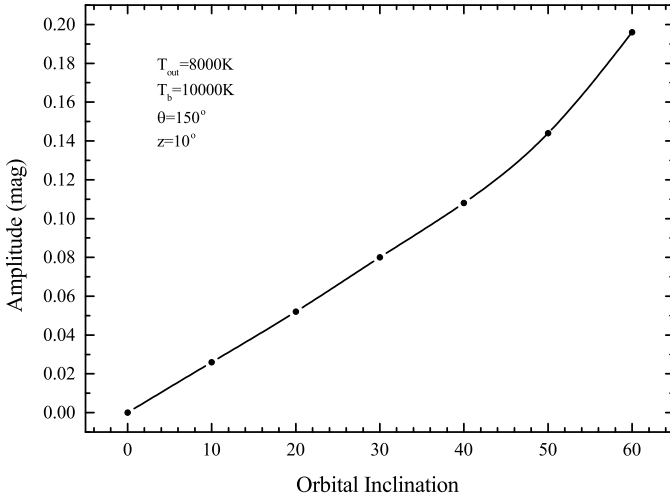


Figure A2. The dependence of the full amplitude of orbital modulation on the orbital inclination.

disc z , and the ratio of temperatures of the bright area and the disc T_b/T_{out} (Fig. A1). The amplitude of light curve decreases quickly with decreasing i (Fig. A2). Our simulations show that for the orbital inclination of 30° the bright area with $T_b=10\,000\text{K}$, $\theta=150^\circ$ and $z=10^\circ$ and the accretion disc with the above parameters creates the modulation with the total amplitude of only 0.08 mag, less than the observed amplitude. Here we claim that these parameters of the bright area are *unrealistic*. They correspond to the blackbody luminosity of the bright area which is twice as large as the total luminosity of the visible half of the accretion disc rim that is not observed in LMXBs or CVs in outbursts. Furthermore, the decrease of the geometrical parameters of the bright area will require to increase this discrepancy further in order to keep the same amplitude of the orbital modulation.

Thus, we conclude that with the use of more or less realistic parameters for the bright area it is nearly impossible to obtain the required orbital variability with the amplitude of at least 0.10 mag for the orbital inclination $i \lesssim 40^\circ$. Only extraordinarily bright and extended area can produce such variability.